24th INTERNATIONAL CONGRESS ON SOUND AND VIBRATION
23–27 July 2017, London

ICSV24
23-27JULY 2017
LONDON CALLING

BOUNDARY LAYER FLOW INTERACTION WITH POROUS SURFACES

Syamir Alihan Showkat Ali and Mahdi Azarpeyvand
Faculty of Engineering, University of Bristol, BS8 1TR, UK
email: ss14494@bristol.ac.uk

Carlos R. Ilário da Silva
Embraer, São José dos Campos, 12227-901, Brazil

The present study demonstrates the mechanisms of flow interaction and sound generation with porous surface as a passive flow control method for different configurations. The flow interaction characteristics have been examined using a flat plate equipped with several surface pressure transducers. To reveal the effect of porosity, four types of porous materials with different porosities and permeability constants were tested. To better understand the effect of flow behaviour over porous surfaces, measurements have been conducted for the boundary layer growth and surface pressure fluctuations, before, over and after the porous section. Velocity measurements have also been performed to investigate the flow pattern and the energy content of the turbulent structure within the boundary layer. Results have shown that the porous surface treatment changes the boundary layer profile and significantly reduces the energy content of the velocity fluctuations within the boundary layer. It has been observed that the porous surface also causes significant reduction in the surface pressure fluctuations of about 6 dB over the high-frequency range. The porous treatment also leads to a noticeable reduction in the coherence and the length-scales of the spanwise flow structures. These results are essential for understanding the flow-porous interaction in real world applications.

1. Introduction

The knowledge of noise generation within a turbulent boundary layer is imperative for flow-induced vibration and noise in many engineering problems and has received extensive consideration in the course of recent years. There are numerous noise control techniques using either passive or active methods. These includes serrations [1–7], morphing [8, 9], porous materials [10–12], surface treatments [13, 14], etc. The passive control methods are more practical and most efficient at mid and higher frequencies [15]. Essentially, amongst the other passive methods, the porous treatments have been of much interest, particularly for this study. Understanding the flow mechanism and noise generation over porous material is not easy as it involves many other dependent parameters such as the roughness, porosity and permeability factor. Contrary to the smooth wall turbulent boundary layer surface pressure fluctuations studies, which have been given a large amount of attention in the last decades [16–19], the rough wall boundary layer surface pressure fluctuations have rather received little attentions.

There have been a few studies on the pressure fluctuations for boundary layers over rough surfaces. Blake [20] studied the pressure fluctuations for turbulent boundary layers over a smooth and a set of three rough walls; the dense-large, sparse-small and dense-small. It is claimed that the different

roughness parameters, such as the roughness separation and height affects the very large-scale structure and small-scale turbulence structure, respectively. It is also found that the coherence lost of the pressure eddies for rough walls are higher than the smooth walls due to the high turbulence production rates near the surface. Varano [21], on the other hand, investigated the rough surface with fetches of hemispherical roughness and found that the TKE and shear stress production increases downstream of the element due to the delay in the flow separation over the top of the element. Also, he confirms that the shear stress reduced almost twice the roughness height away from the wall, which is associated to the high mean velocity gradient at that particular location. A recent effort by Meyers *et al.* [22] shows a comprehensive studies on wall pressure spectrum of a flat plate with smooth and rough walls (sparse arrays of different size and distribution of hemispherical bumps) at high Reynolds numbers. They showed that the boundary layers of both the rough and smooth surfaces have similar scales on the outer boundary layer at the low frequencies of the wall-pressure spectrum, and has a universal viscous form at the higher frequency range. They also confirms that the friction velocity obtained from the rough-wall boundary layers is always less than the conventional friction velocity achieved by the smooth-wall boundary layers and affirmed that the boundary layer parameters and the wall pressure spectrum are nearly independent of the surface roughness for the conditions considered in their study. Building on the work of Meyers, Liselle *et al.* [23] have investigated rough walls with two etches of hemispherical roughness with two different sparseness ratio. They demonstrated that the pressure spectral shape changes at mid frequencies with the roughness density, and it was speculated that the spectral changes are not due to the changes in the turbulence structure but rather due to the displacement of the pressure fluctuations over the roughness elements.

There have been no proper studies presented on the porous-typed rough wall pressure fluctuations, and more importantly, the effect of such surfaces on the turbulence-generated noise and boundary layer due to the scrubbing of the flow past the porous surface has been investigated in this paper. This paper aims to provide a comprehensive study on the effects of porous surfaces on the boundary layer development, surface pressure fluctuations and noise generation. The experimental setup and wind-tunnel tests are described in Sec. 2. The results and discussions are detailed in Sec. 3.

2. Measurement Setup

The present experiments have been conducted for a flat plate, with solid and porous surfaces, in the open jet wind tunnel of the University of Bristol. The wind tunnel has a test-section with a diameter of 1 m and with length of 2 m. The measurements were performed for flow velocity of 20 m/s with a maximum flow turbulence intensity of 0.05 %. The general layout of the experimental setup is shown in Fig. 1(a). The plate has a length of 1265 mm and a spanwise length of 715 mm, with an elliptical leading edge in order to prevent flow separation and strong adverse pressure gradient at the beginning of the plate. To ensure a zero-pressure gradient turbulent boundary layer on the topside of the plate, particularly near to the trailing-edge, a 12° beveled trailing-edge was employed [24]. A 50 mm wide sand trip was applied just after the leading edge to ensure a well-developed turbulent flow before the porous section. The porous section is placed at the mid-span, 315 mm upstream of the trailing-edge with a width, length and height of 200 mm, 120 mm and 10 mm, respectively. Four metal foams with the PPI (pores per inch) of 25, 35, 45 and 80 were used for this study. The plate was instrumented with 32 FG-23329-P07 miniature transducers for the measurement of the unsteady boundary layer surface pressure fluctuations. The transducers are 2.5 mm in diameter and have a circular sensing area of 0.8 mm and were positioned under a pinhole mask of 0.4 mm diameter in order to compensate the large discontinuities [25] of the pressure attenuation at the wall [26]. The transducers were installed inside the plate parallel to the surface and were located at the porous section and the solid surface, upstream and downstream of the porous section in streamwise and spanwise directions. The layout of the transducers location on the plate is shown in Fig. 1(b) and summarized in Table 1. The surface pressure fluctuations data has been acquired by a National Instrument PXIe-

4499, with a sampling frequency of 2^{16} Hz and measurement time of 32 seconds. In order to measure the turbulent properties of the flow, the boundary layer measurements were carried out using a single hot-wire Dantec 55P16 probe, with a platinum-plated tungsten wire of 5 μm diameter and 1.25 mm length. A Dantec StramlinePro frame with CTA91C10 module was used to operate the probe and the probe was calibrated using the Dantec 54H10 type calibrator. The signals were low-pass filtered by the StramlinePro with a corner frequency of 30 kHz before they were A/D converted, with an applied overheat ratio of 0.8 [27]. The hot-wire data was acquired by a National Instrument 9215 type device, with a sampling frequency of 40 kHz and the signals were recorded for 8 seconds at each location.

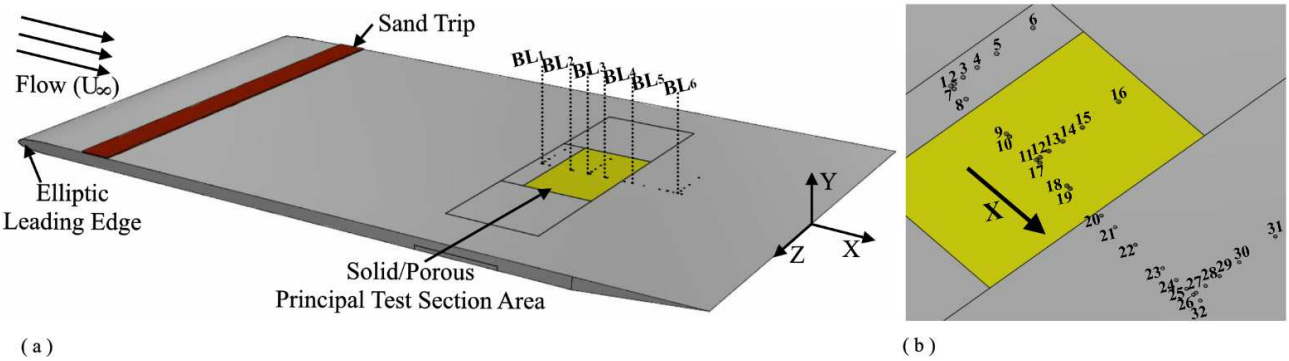

Figure 1: Flat plate test rig (a) Scrubbing flat plate experimental setup and (b) Positions of pinholes transducers

Table 1: Positions of the pinhole transducers on the plate

Position	**Section/ Boundary**	**Transducer Number,** p	**Axial locations,** x (mm)	**Transverse locations,** z (mm)
Streamwise	Solid	1, 7, 8	460, 456.8, 445	0.0
	Porous	9, 10, 11, 17, 18, 19	405, 401.8, 375, 371.8, 345, 341.8	
	Solid	20, 21, 22, 23, 24, 25, 26, 32	310.75, 297.25, 277, 250, 236.5, 226.38, 219.63, 212.88	
Spanwise	Solid	1, 2, 3, 4, 5, 6	460	0, 3.2, 11.4, 24.4, 42.6, 76.4
	Porous	11, 12, 13, 14, 15, 16	375	
	Solid	26, 27, 28, 29, 30, 31	219.63	

3. Results and Discussion

To better understand the effect of turbulence-generated noise due to the scrubbing of the flow past a porous flat surface, the boundary layer velocity profile and their energy content results are given in this section. Further discussions on the pressure power spectrum, lateral coherence and the spanwise length scale over the flat plate will also be presented. The measurements are conducted at free-stream velocity of U_∞=20 m/s.

3.1 Boundary Layer Velocity Profile and Their Energy Content

The fundamental understanding of the flow behaviour over a flat plate is essential to analyze the flow characteristics past the porous surface. Figure 2 presents the mean and root-mean-square (rms) boundary layer velocity profiles along the streamwise boundary layer lines (BL_1-BL_6), shown in

Fig. 1 (a). The measurement locations are taken over the test section area (solid and porous), and at the region upstream and downstream of the surface treatment section to get the whole picture of the boundary layer transition trend. The y-axis of the boundary layer profiles were normalized with the solid (baseline) boundary layer thickness at each measurement locations. This is because, the velocity of the fluid approaches to zero at the solid surface, resulting in no-slip condition, which will not be the case over the porous surface due to the flow penetration into the porous structure. As expected, the mean velocity profiles at BL_1, upstream of the test section are found to be similar for all cases. It is noticed that all of the boundary layer profiles downstream from BL_1 change for all cases. There is a decrease in the velocity gradient for the porous cases (especially for the case of porous 25 PPI) at the wall from BL_2 to BL_6 and the boundary layer thickness is found to be increasing from BL_2 to BL_6, due to the deceleration of the flow at the plate surface. The variation in the velocity gradient between the porous cases and solid, however, becomes smaller at the further downstream locations of the plate, from BL_5 to BL_6. The rms velocity profiles, on the other hand, clearly shows that the whole energy cascade of the boundary layer has changed significantly. It can be seen that the rms velocity magnitude near the wall region for all cases, especially for the case of porous 25 PPI increases quickly, as the flow past over the porous region (BL_2 to BL_4) and reduces slowly at the downstream solid region (BL_5 to BL_6). The increase in the energy content of the velocity fluctuations in the vicinity of the porous surface can be attributed to the frictional forces due to the rough surface of the material. Despite the energy content increase near the porous surface, it can be seen that the energy content of the larger turbulence structures are reduced with the porous surface treatment at almost below the boundary layer thickness ($0.4 \lesssim y/\delta_o \lesssim 1$), for all locations downstream of BL_1. Interestingly, the largest reduction of the energy content is seen for the case of porous 80 PPI material. From the results presented in Fig. 2, one can conclude that the use of porous materials can lead to an increase of the wall shear stress and thus intensify the turbulent pressure fluctuations in the boundary layer but significant reduction of the turbulent structures energy content data within the boundary layer. The results obtained is particularly important as the energy content demonstrate the relationship between the large coherent structures in the log-law and outer layer regions and the noise generation, indicating the possibilities of noise reduction using porous surfaces. The underlying effect of the porous material on the flow behaviour and noise generation can be further analyzed with the boundary layer surface pressure fluctuations information, which will be dealt with in subsection 3.2 and 3.3.

3.2 Wall Pressure Power Spectra

In order to characterize the scrubbing noise effect on the flat plate, it is necessary to examine the pressure exerted on the surface with and without the porous treatment. Figure 3 presents the point spectra of the surface-pressure fluctuations $\phi_{pp}(f)$, obtained from the transducers $p1$, $p11$, $p18$ and $p26$. The captured $\phi_{pp}(f)$ for all cases are quite similar to each other at x=-460 mm ($p1$), upstream of the test section in the lower frequency region, with slight reduction of the surface pressure fluctuations at the higher frequency region. It has been observed that the porous treatment increases the broadband energy content in the frequency range between 200 and 3000 Hz over the porous surface, which is believed to be due to the frictional forces between the rough porous surface and the flow. Also, the emergence of a small broadband peak between f= 200 to 400 Hz can be seen at the same locations, especially for the lower PPI porous material (25, 35 and 45 PPI), which can be attributed to the existence of localized strong hydrodynamic field and flow circulation inside the porous medium [28]. The broadband peak, however, dissipates very quickly at further downstream locations, after the test section ($p26$). Interestingly, the results have also shown that a very strong reduction of ϕ_{pp} will be achieved after the porous section ($p26$) over the high frequency range, $f >$ 7000 Hz, for all the porous cases. Notably, the 25 PPI material leads to the highest reduction of the surface pressure fluctuations by up to 6 dB or more at the high frequency regions.

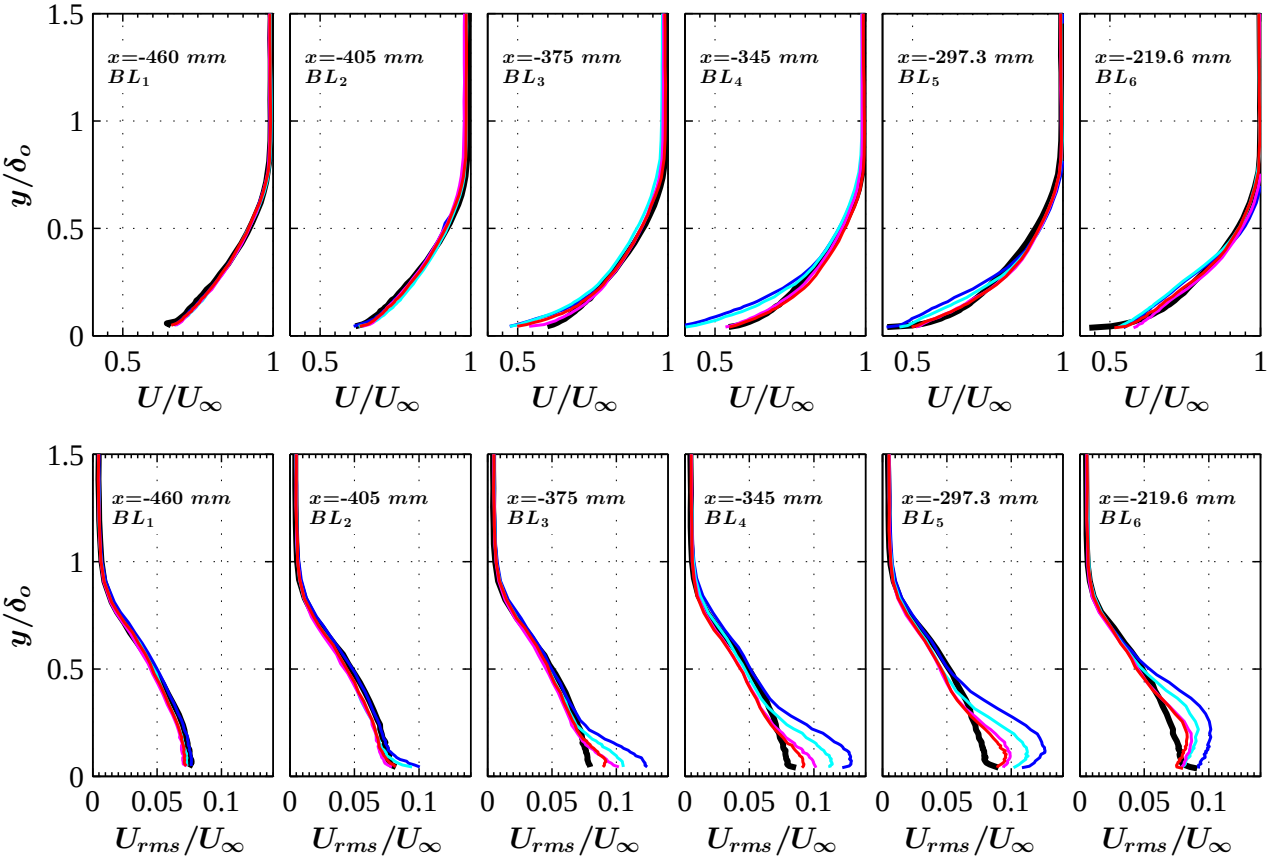

Figure 2: Boundary layer mean and RMS velocity profiles at different streamwise locations over the flat plate. *Solid(——), Porous 80 PPI(——), Porous 45 PPI(——), Porous 35 PPI(——), Porous 25 PPI(——)*

3.3 Lateral Coherence and Length-scales

The stochastic character of the turbulent structures can be further evaluated using the average spatial extent (coherence) of the surface pressure fluctuations. Figure 4 presents the lateral coherence $\gamma^2(f)$, measured between all the six spanwise transducers $p11$ to $p16$ at x=-375 mm and $p26$ to $p31$ at x=-219.6 mm for solid (baseline) and two porous cases with 25 and 80 PPI materials. The spanwise correlation length $\Lambda_{p,3}$, obtained from the coherence of the pressure fluctuations are illustrated in Fig. 5. The γ^2 and $\Lambda_{p,3}$ obtained for the spanwise transducers at x=-460 mm (upstream of the test section) are similar for all the cases, and therefore is not presented in this section. Figure 4 clearly shows that the porous treatment has strong impact on the coherence of the flow structures over the test section region, x=-375 mm. Also, it can be seen that γ^2 (Fig. 4 (b)) and $\Lambda_{p,3}$ (Fig. 5 (a)) for porous 80 PPI at x=-375 mm, are reduced much faster with Δz than the solid (baseline). On the contrary, porous 25 PPI has eliminated the coherent structures of the flow for the spacing distance Δz > 11.4 mm, as the eddies became independent of each other. However, similar to the findings in Fig. 3, the emergence of a broadband peak can be seen at the same frequency region between f= 200 Hz to 400 Hz (see Fig 3), for the spacing distance, Δz of 3.2 mm and 11.4 mm. The spanwise length-scales, $\Lambda_{p,3}$ (Fig. 5 (a)), on the other hand, remain steady, with a little hump over the same frequency region and effectively reduced at the higher frequency region, f>600 Hz. Immediately downstream of the test section (x=-219.6 mm), the coherence behaviour for porous 80 PPI changes completely, with the γ^2 and $\Lambda_{p,3}$ of the flow structures increasing significantly, larger than the results obtained at x=-375 mm. Similar observations have been made for the case of porous 25 PPI where the γ^2 and $\Lambda_{p,3}$ increases at low frequencies for all transducer distances, Δz. It is clear that the porous surface

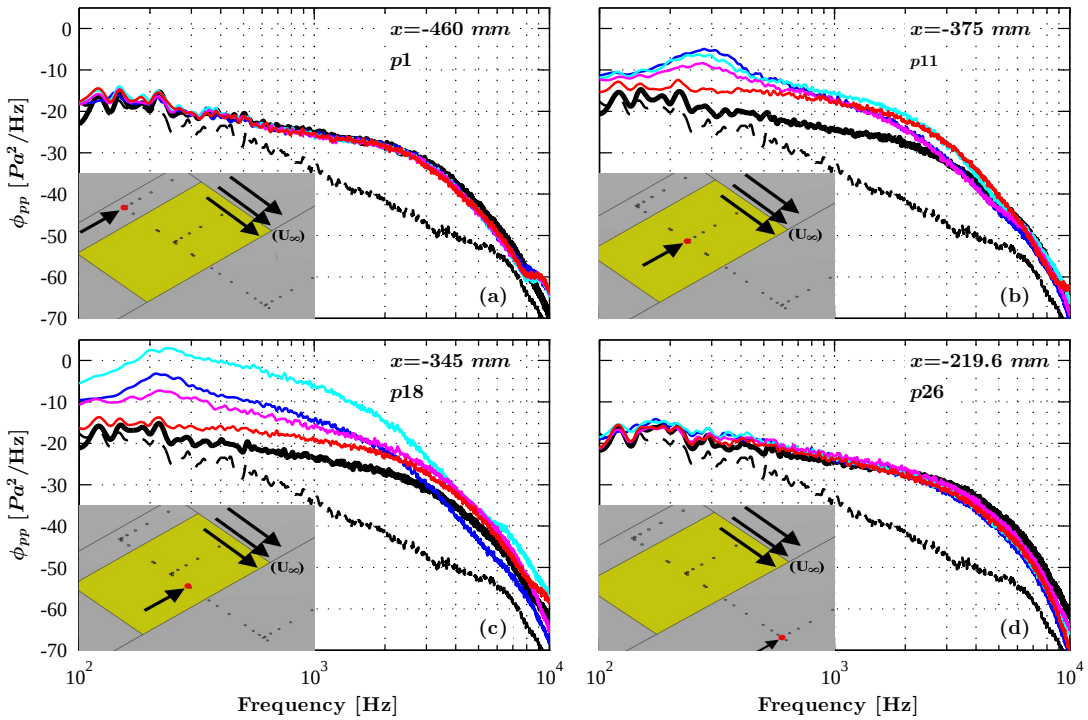

Figure 3: Point spectra of pressure fluctuations at different streamwise locations over the flat plate. *Background noise(- - - - -), Solid(———), Porous 80 PPI(—), Porous 45 PPI(—), Porous 35 PPI(—), Porous 25 PPI(—)*

treatment significantly changes the coherence and length-scales of the surface pressure fluctuations at the low frequency range and completely eliminates the pressure fluctuations at high frequency range, especially for the 25 PPI treated case.

4. Conclusion

The investigation of turbulence-generated noise due to the scrubbing of the flow past a flat porous surface has been addressed in this study. Results have shown that the use of porous surface treatments leads to an increase in the energy content of the velocity fluctuations near the surface but significantly reduces the energy content of the larger turbulent structure within the boundary layer. It is also obvious that the porous surface treatment has noticeably reduced the power spectral density of the surface pressure fluctuations in the high-frequency range. Furthermore, results have shown that porous treatments are efficient in reducing the coherence and the length-scales in the spanwise direction over the test-section region. Results have shown that the use of a rough and permeable surface, leads to the emergence of complex turbulence structures, potentially leading to reduction of generated noise, whose understanding will require more in-depth studies.

5. Acknowledgement

This project is sponsored by Embraer S.A. . The second author (MA) would like to acknowledge the financial support of the Royal Academy of Engineering.

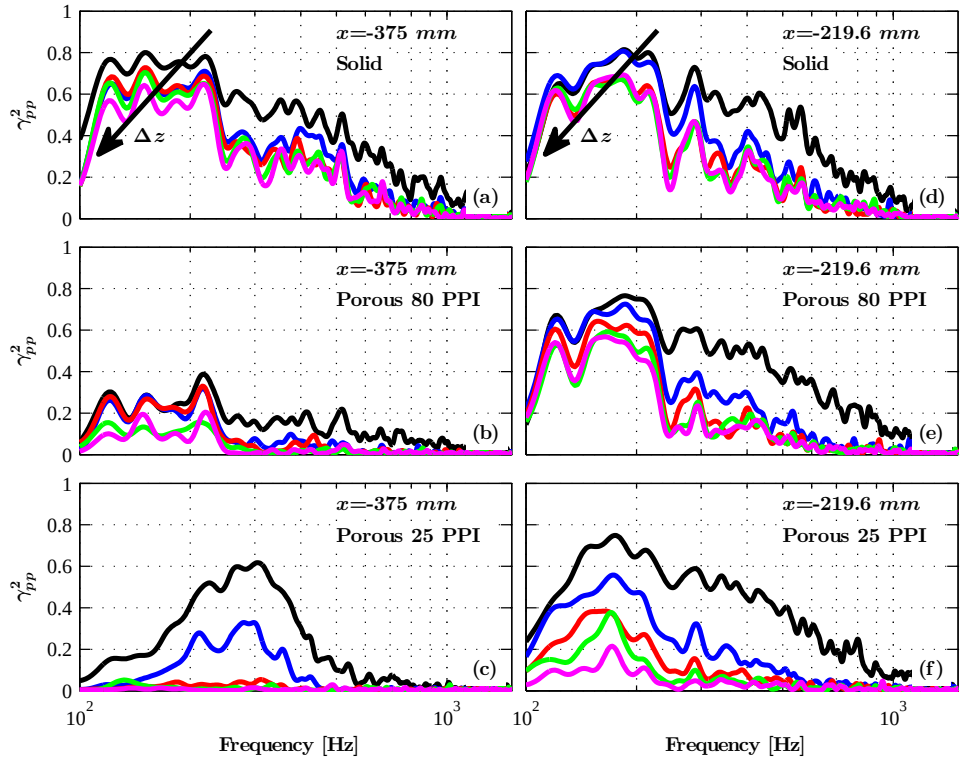

Figure 4: Lateral coherence between spanwise transducers at x=-375 mm (a,b,c) and x=-219.6 mm (d,e,f). Δz=*3.2 mm(——), Δz=11.4 mm(——), Δz=24.4 mm(——), Δz=42.6 mm(——), Δz=76.4 mm(——)*

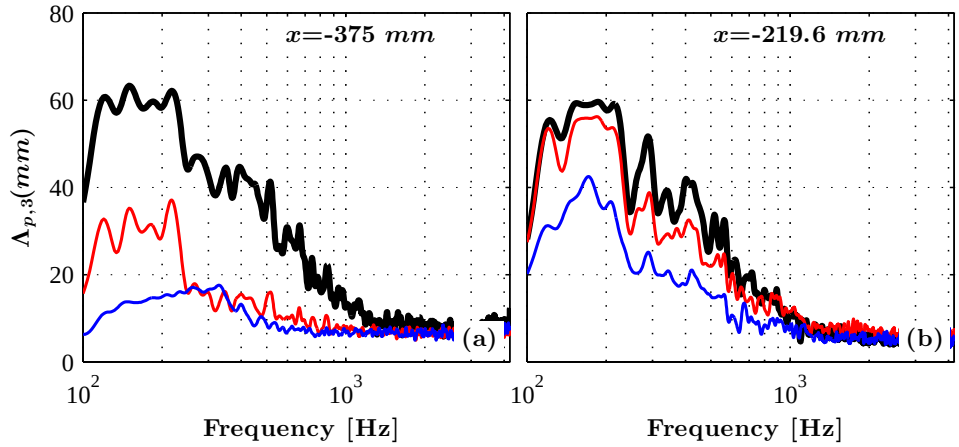

Figure 5: Spanwise length-scales at x=-375 mm (a) and x=-219.6 mm (b). *Solid(——), Porous 80 PPI(——), Porous 25 PPI(——)*

References

1. Liu, X., Kamliya Jawahar, H., Azarpeyvand, M. and Theunissen, R. Wake development of airfoils with serrated trailing edges, *22nd AIAA/CEAS Aeroacoustics Conference*, p. 2817, (AIAA 2016-2817).

2. Liu, X., Azarpeyvand, M. and Theunissen, R. Aerodynamic and aeroacoustic performance of serrated airfoils, *21st AIAA/CEAS Aeroacoustics Conference*, p. 2201, (2015).

3. Lyu, B., Azarpeyvand, M. and Sinayoko, S. Prediction of noise from serrated trailing edges, *Journal of Fluid Mechanics*, **793**, 556–588, (2016).

4. Lyu, B., Azarpeyvand, M. and Sinayoko, S. A trailing-edge noise model for serrated edges, *21st AIAA/CEAS Aeroacoustics Conference*, p. 2362, (AIAA 2015-2362).
5. Azarpeyvand, M., Gruber, M. and Joseph, P. An analytical investigation of trailing edge noise reduction using novel serrations, *19th AIAA/CEAS aeroacoustics conference*, (AIAA 2013-2009).
6. Gruber, M., Azarpeyvand, M. and Joseph, P. F. Airfoil trailing edge noise reduction by the introduction of sawtooth and slitted trailing edge geometries, *20th International Congress on Acoustics*, **10**, 6, (2010).
7. Gruber, M., Joseph, P. and Azarpeyvand, M. An experimental investigation of novel trailing edge geometries on airfoil trailing edge noise reduction, *19th AIAA/CEAS Aeroacoustics Conference*, (A1AA 2013-2011).
8. Ai, Q., Azarpeyvand, M., Lachenal, X. and Weaver, P. M. Aerodynamic and aeroacoustic performance of airfoils with morphing structures, *Wind Energy*, (Vol. 19, No. 7, 2016, pp. 1325-1339).
9. Ai, Q., Weaver, P. and Azarpeyvand, M. Design optimization of a morphing flap device using variable stiffness materials, *24th AIAA/AHS Adaptive Structures Conference*, p. 0816, (AIAA 2016-0816).
10. Showkat Ali, S. A., Szoke, M., Azarpeyvand, M. and Ilário, C. Trailing edge bluntness flow and noise control using porous treatments, *22nd AIAA/CEAS Aeroacoustics Conference*, p. 2832, (AIAA 2016-2832).
11. Showkat Ali, S. A., Liu, X. and Azarpeyvand, M. Bluff body flow and noise control using porous media, *22nd AIAA/CEAS Aeroacoustics Conference*, p. 2754, (AIAA 2016-2754).
12. Liu, H., Azarpeyvand, M., Wei, J. and Qu, Z. Tandem cylinder aerodynamic sound control using porous coating, *Journal of Sound and Vibration*, **334**, 190–201, (2015).
13. Afshari, A., Azarpeyvand, M., Dehghan, A. A. and Szoke, M. Trailing edge noise reduction using novel surface treatments, *22nd AIAA/CEAS Aeroacoustics Conference*, p. 2834, (AIAA 2016-2384).
14. Afshari, A., Dehghan, A. A., Azarpeyvand, M. and Szőke, M. Three-dimentional surface treatments for trailing edge noise reduction, *22nd AIAA/CEAS Aeroacoustics Conference*, (AIAA 2016-2384).
15. Tiseo, B., et al. Passive-active noise control of an acoustic duct, *Journal of Theoretical and Applied Mechanics*, **49** (4), 1135–1149, (2011).
16. Bradshaw, P. ŚinactiveŠmotion and pressure fluctuations in turbulent boundary layers, *Journal of Fluid Mechanics*, **30** (02), 241–258, (1967).
17. Bull, M. Wall-pressure fluctuations associated with subsonic turbulent boundary layer flow, *Journal of Fluid Mechanics*, **28** (04), 719–754, (1967).
18. Farabee, T. M. and Casarella, M. J. Spectral features of wall pressure fluctuations beneath turbulent boundary layers, *Physics of Fluids A: Fluid Dynamics*, **3** (10), 2410–2420, (1991).
19. Goody, M. Empirical spectral model of surface pressure fluctuations, *AIAA journal*, **42** (9), 1788–1794, (2004).
20. Blake, W. K. Turbulent boundary-layer wall-pressure fluctuations on smooth and rough walls, *Journal of Fluid Mechanics*, **44** (04), 637–660, (1970).
21. Varano, N. D., *Fluid dynamics and surface pressure fluctuations of turbulent boundary layers over sparse roughness*, Ph.D. thesis, Virginia Tech, (2010).
22. Meyers, T., Forest, J. B. and Devenport, W. J. The wall-pressure spectrum of high-reynolds-number turbulent boundary-layer flows over rough surfaces, *Journal of Fluid Mechanics*, **768**, 261–293, (2015).
23. Joseph, L. A., Meyers, T. W., Molinaro, N. J. and Devenport, W. J. Pressure fluctuations in a high-reynolds-number turbulent boundary layer flow over rough surfaces, *22nd AIAA/CEAS Aeroacoustics Conference*, p. 2751, (AIAA 2016-2751).
24. Mosallem, M. Numerical and experimental investigation of beveled trailing edge flow fields, *Journal of Hydrodynamics, Ser. B*, **20** (3), 273–279, (2008).
25. Bull, M. and Thomas, A. High frequency wall-pressure fluctuations in turbulent boundary layers, *Physics of Fluids (1958-1988)*, **19** (4), 597–599, (1976).
26. Corcos, G. Resolution of pressure in turbulence, *The Journal of the Acoustical Society of America*, **35** (2), 192–199, (1963).
27. A/S, D. D., *Dantec Dynamics StreamWare Pro Installation and User Guide*, 5.11.00.14., 9040U4931 (2013).
28. Das, D., Nassehi, V. and Wakeman, R. A finite volume model for the hydrodynamics of combined free and porous flow in sub-surface regions, *Advances in Environmental Research*, **7** (1), 35–58, (2002).